https://doi.org/10.26599/FRICT.2026.9441339

Research Article

Atomic level manufacturing enables ultra-low friction and wear at elevated temperatures

Shehui Dang[1], Lei Chen[1,*], Pengfei Shi[2], Runzi Wang[1], Wumao Peng[1], Liang Jiang[1], Andreas Rosenkranz[3,4], Linmao Qian[1]

[1] *Atomic Level Manufacturing Center, School of Mechanical Engineering, Southwest Jiaotong University, Chengdu, China*

[2] *School of Mechatronics and Vehicle Engineering, Chongqing Jiaotong University, Chongqing, China*

[3] *Department of Chemical Engineering, Biotechnology and Materials, FCFM, University of Chile, Santiago 8370415, Chile*

[4] *ANID – Millennium Science Initiative Program, Millennium Nuclei of Advanced MXenes for Sustainable Applications (AMXSA), Santiago, 8370415, Chile*

Corresponding author: chenlei@swjtu.edu.cn (Lei Chen)

Received: April 27, 2026; Revised: November 5, 2026; Accepted: November 18, 2026

© The Author(s) 2026.

Just Accepted

Abstract

Toward the goal of achieving ultra-low friction and wear under elevated temperatures and high contact pressures in industrially relevant mechanical systems relying on liquid lubrication, we propose a synergistic lubrication strategy that integrates a close-to-atomically smooth surface as well as atomic-level modifications using a MXene coating and [HMIM][BF_4] ionic liquid (IL). The ball-on-disc tribological test results demonstrate that this strategy led to ultra-low friction and wear of engineering steel interfaces at a high contact pressure of 1.13 GPa and

an elevated temperature of 300 °C, demonstrating competitive lubrication performance relative to reported traditional oil-based and IL-based lubrication systems. The underlying mechanism enabling the superlative performance is attributed to a solid-liquid synergy since the close-to-atomic smooth steel surface not only mitigates direct load-bearing asperity contact at the sliding interface but also enhances the adhesion of MXenes to form a thicker, uniform composite tribofilm. In contrast, a higher steel roughness induces interfacial stress concentrations, leading to film delamination and failure. This template of lubrication strategy is anticipated to overcome the failure challenge of conventional liquid lubrication in extreme environments and provide a foundational roadmap for designing ultra-low friction and wear sliding systems operating under high-contact-pressure, high-temperature conditions relevant to industrial applications.

Keywords**:** Ultra-low friction; MXenes; Ionic liquid; Atomic-level polishing; High temperature; Liquid lubrication

Just Accepted

1. Introduction

Ultra-low friction and ultra-high wear resistance under extreme load and temperature conditions are pivotal for the reliability and energy efficiency of advanced mechanical systems, which include high-speed spindles in ultra-precision machining, sliding bearings in aerospace actuators, and gear trains in high-temperature operating environments [1-5]. In these regimes, conventional liquid lubricants (mineral oils, synthetic esters, among others) undergo thermal oxidation, viscosity loss and film breakdown, while additives tend to suffer from tribo-oxidation or structural collapse, leading to a rapid increase in friction and catastrophic wear [6-11]. These limitations highlight the urgent need for alternative strategies that go beyond conventional liquid lubrication, particularly through precise design of tribological interfaces at the atomic scale to achieve high-performance lubrication [12-15].

Ultra-precision polishing has matured to create surface finishes with atomic roughness and nanometric form accuracy [16-18], notably reducing asperity contact and enabling new regimes of mixed and elastohydrodynamic lubrication [19, 20]. Parallel advances in atomic-level polishing, atomic-level modification such as atomic layer deposition, layer-by-layer assembly and two-dimensional (2D) material engineering allow for the design of functional coatings with atomic-scale thickness control, tailored crystallinity and surface chemistry [14, 21]. Atomically smooth substrate surfaces enable the controlled deposition of 2D materials via solution processing or vapor-phase methods, producing lamellar coatings with tunable interlayer spacing, functional terminations and high thermal stability [22-24]. Such well-designed solid surfaces with lamellar coatings enable effective integration with high-performance liquid lubricants, particularly ionic liquids (IL), whose excellent thermal stability, tunable molecular structures, and strong interfacial interactions effectively modulate surface modification and tribological interface interaction [25-30]. Consequently, atomic-level manufacturing helps to redefine tribological interfaces by precisely orchestrating mechanical, chemical and structural interactions at the nanometer scale and even atomic scale [31, 32]. However, the underlying synergistic mechanisms between atomic-level polishing and modification are poorly understood, hindering the prediction and optimization of its impact on the resulting tribological performance [33, 34]. Critical questions persist regarding how surface

Just Accepted

topography influences adhesion, continuity and tribochemical evolution of 2D coatings, and how these solid layers synergize with liquid films to sustain lubrication at elevated temperatures. Addressing these gaps is crucial for the rational design of robust and durable ultra-low friction systems in extreme manufacturing.

This paper reports a simple synergistic lubrication strategy combining [HMIM][BF_4] IL and MXenes ($Ti_3C_2T_x$) coatings, synergized with close-to-atomic scale smooth surface manufacturing that resulted in an exceptional lubricity performance and wear resistance under high contact pressures of ~1.1 GPa and elevated temperature of 300 °C. The detailed characterization of the tribological interface revealed the origin of such superlative performance in the interplay between surface roughness, lubrication regimes, and tribo-chemical reactivity. Optical profilometry, transmission electron microscopy (TEM), energy dispersive X-ray spectroscopy (EDS) and X-ray photoelectron spectroscopy (XPS) were used to quantify the properties and delineate the phenomenon. Moreover, molecular dynamics (MD) simulations were used to complement these analyses by qualitatively probing the roughness-dependent interfacial contact and deformation behaviors of MXene at atomic scale. Our findings may open a new avenue for designing ultra-low friction and wear sliding systems operating under high-contact-pressure, high-temperature conditions relevant to industrial applications.

2. Experimental materials and methods

2.1 Materials preparation

18CrNiMo7-6 gear steel substrates (with a dimension of 10 mm × 10 mm × 3 mm) and GCr15 bearing steel balls (6 mm in diameter) were used as tribo-pairs. The initial surface roughness of the balls was S_a = 3.20 ± 0.43 nm measured by White-light interferometry (WLI) (**Fig. S1**). $Ti_3C_2T_x$ nanoflakes, with a purity of 96%, were purchased from Nanjing XFNANO Materials Tech. Co., Ltd., China. Excessively large MXene nanoflakes may hinder their transport into highly confined contact regions, whereas excessive size reduction may compromise their dispersion stability and uniform coating formation [35-38]. Therefore, the MXene nanoflakes used in this study exhibited a moderate average lateral size of

Just Accepted

approximately 3277 ± 1233 nm. These nanoflakes could be readily deposited by drop-casting to form a relatively uniform coating with limited agglomeration (**Fig. S2**).

The gear steel substrates were first ultrasonically cleaned in ethanol and deionized water for 10 min each, followed by drying with nitrogen gas to obtain clean substrate surfaces. To minimize nanoflake aggregation and improve dispersion, MXene nanoflakes were dispersed in anhydrous ethanol and ultrasonicated for 30 min to prepare a suspension with a concentration of approximately 5 wt%. Subsequently, the 100 μL suspension was drop-cast onto the cleaned gear steel substrates, followed by drying in a laminar-flow cabinet at room temperature (RT) for 12 h. The substrate cleaning procedure, MXene concentration, and drying conditions were kept consistent for all specimens. White-light interferometry (WLI) measurements of 50 specimens yielded an average coating thickness of 24.35 μm, with 70% of the values distributed between 21.8 and 27.9 μm **(Fig. S2)**, demonstrating good reproducibility of the coating preparation. Commercial 1-hexyl-3-methylimidazolium tetrafluoroborate ionic liquid ([HMIM][BF_4] IL) with a purity of 97% from Aladdin Reagent Co., Ltd., Shanghai, China was used as base lubricant.

2.2 Chemical mechanical polishing

Chemical mechanical polishing (CMP) process was used to prepare 18CrNiMo7-6 steel with different surface roughness ranging from 795 to 1.8 nm. Three pieces of 18CrNiMo7-6 steel were simultaneously polished by an automatic pressure lapping/polishing machine (UNIPOL-1200S, Shenyang Kejing Automatic Equipment Co., Ltd., Shenyang, Liaoning, China). Polyurethane polishing pad (IC1010/Suba IV) was used. For the CMP slurry, the involved colloidal silica (YZ8040) was purchased from Shanghai YZ-Lapping Material Co., Ltd (Shanghai, China). The complexing agents including formic acid, oxalic acid or citric acid were purchased from Sinopharm Chemical Reagent Co., Ltd. (Shanghai, China), while other compositions include oxidant (H_2O_2) and pH buffer (HNO_3 and KOH). After polishing, the samples were thoroughly cleaned and dried.

The CMP process was conducted under an applied load of 1.35 kg, corresponding to a

Just Accepted

nominal contact pressure of approximately 6.40 psi (44.1 kPa), with both the carrier and platen rotating at 60 rpm. The polishing slurry consisted of 2 wt% silica abrasives, 1 wt% H_2O_2, and 0.067 mol/L citric acid, thus maintaining a pH of 3. Under these polishing conditions, superficial iron is initially oxidized by H_2O_2 to Fe^{2+} and Fe^{3+}, which subsequently reacts with citric acid to form FeHCit and FeCit. This outermost reaction layer serves a dual purpose since it passivates the surface to inhibit corrosion and is readily removed by polishing abrasives, enabling atomic-level finishing [18]. Different gear steel substrates with varying surface roughness were obtained by varying the polishing duration while maintaining the same CMP conditions.

2.3 Tribological testing

The ball-on-disc tribological tests were carried out using a universal commercial tribometer (UMT TriboLab, Bruker, USA) equipped with a temperature controller in rotational mode. The rotational speed and radius are 150 rpm and 1.5 mm, respectively, thus adjusting a linear speed u of 0.024 m/s. The applied normal force F_n was 5 N, resulting in an initial (maximum) Hertzian contact pressure of 1.13 GPa [39].

Prior to tribo-testing, the tribo-pairs were sonicated in ethanol and pure water for 10 min and then dried with nitrogen. The tribological tests were conducted at RT (23 ± 2 ℃), 100, 200, 300, and 400 ℃, respectively. The heating rate was 12.5 ℃/min. After reaching the target temperature, it was maintained for 3 min before starting the experiment. Before heating, 50 μL of the IL was pre-introduced into the contact zone to ensure sufficient lubricant supply to the sliding interface, and the same volume was used for all tests to exclude the influence of lubricant quantity on the comparison of tribological performance. Considering the relatively large coefficient of friction (COF) fluctuations during the initial 600 s running-in stage, the average steady-state COF was evaluated over the subsequent 600–3600 s interval. All experiments were repeated at least three times to ensure reproducible testing results.

For the bearing steel balls, the wear scar diameter d was measured using an optical microscope (Axio Lab A1, Zeiss, Germany). Assuming that the wear scar corresponds to a spherical cap, the wear depth h_b, was calculated as:

Just Accepted

$$h_b = r_b - \sqrt{r_b^2 - \frac{d^2}{4}} \quad (1)$$

where r_b is the radius of the ball. The corresponding wear volume of the ball V_b was then calculated from the spherical-cap geometry:

$$V_b = \left(\frac{\pi h_b}{6}\right)\left(\frac{3d^2}{4} + h_b^2\right) \quad (2)$$

The specific wear rate K_b of the bearing steel ball was calculated according to Archard's relationship, $K_b = V_b/F_nS$ [40], where S is the total sliding distance. For the gear steel substrates, the wear-track topography was characterized using WLI. The cross-sectional area of the wear track A was extracted from the measured profiles. Following the same approach used for the bearing steel ball, the specific wear rate K_d of the disc substrate was subsequently calculated as: $K_d = AL/F_nS$, where L is the length of the wear track, and AL represents the wear volume of the gear steel substrate.

2.4 Materials Characterization

With respect to MXene nanoflakes, the particle size distribution was determined using a particle size analyzer (Litesizer 500, Anton Paar, Austria). The MXene nanoflakes were dispersed in ethanol and then dripped onto a copper grid to obtain the morphology using field-emission transmission electron microscopy (FE-TEM; Talos F200S G2, Thermo Fisher Scientific, USA). The structural features of the nanoflakes were investigated using Raman spectroscopy (DXR2xi, Thermo Fisher Scientific, USA) averaging 5 accumulations, integration time of 3 s, excitation wavelength of 785 nm, and 5% of the maximum laser intensity. The phase structures of the MXene nanoflakes were investigated by X-ray diffraction (XRD; D8 Advance, Bruker, USA) using 40 kV and 40 mA with Cu Kα radiation (λ = 0.15406 nm).

For [HMIM][BF_4] IL, the thermal stability was analyzed using thermogravimetric analysis (TGA; TGA4000, Perlcin Elmer, USA) with a heating rate of 10 °C/min in the nitrogen

Just Accepted

atmosphere. The temperature-dependent dynamic viscosity was measured using a rotational rheometer (HAAKE MARS 60, Thermo Fisher Scientific, Germany) equipped with a 20 mm concentric-cylinder measuring geometry at a constant shear rate of 500 s^{-1} over the temperature range of 25 – 300 °C. WLI was used to characterize surface roughness, coating thickness and worn surface topography. After testing, the chemical composition in wear tracks was measured using X-ray photoelectron spectroscopy (ESCALAB 250XI, Thermo Scientific, USA) with non-monochromatic Al Kα radiation. The XPS measurements were realized using Avantage software, which applied the "Smart" method for background correction and Gaussian-Lorentzian curve fitting. The binding energies were calibrated with C_{1s} at 284.6 eV.

2.5 MD simulation

To investigate the influence of the surface roughness on the interfacial contact behavior between the MXene flakes and the substrate at the atomic scale, this study conducted MD simulations. We constructed a physical model consisting of a single-layer $Ti_3C_2T_x$ and a series of carbon substrates with different sinusoidal undulation heights (R_z = 0 - 4 nm). The inter-atomic interactions were described by the Tersoff potential [41]. The time step of 0.5 fs was used in all simulations, while periodic boundary conditions were applied in x- and y-directions. The NVT ensemble was used during all simulations, while the system temperature was controlled by a Berendsen thermostat applied to the thermostat layers. All calculations were performed by using the open-source LAMMPS code [42]. All atomic trajectories were analyzed using the OVITO software [43]. The present model was intentionally simplified to probe the roughness-dependent interfacial retention behaviors of MXene. Given the chemical and structural complexity of the actual steel/MXene/IL tribological interface, reproducing the complete experimental system at the atomistic scale is computationally prohibitive and beyond the scope of the present simulation.

Just Accepted

3. Results and Discussion

3.1 Ultra-low friction achieved via atomic-level modification and polishing

The tribological tests at elevated temperatures (**Fig. 1**a) were carried out between GCr15 bearing steel ball and 18CrNiMo7-6 gear steel substrate under atomic-level modification with thermally stable [HMIM][BF_4] IL (dynamic viscosity at 300 ℃: 2.95 mPa·s, **Fig. 1**b; decomposition temperature: ~420.1 ℃, **Fig. S3** in SI) and coated $Ti_3C_2T_x$ MXene lamellar materials (interlamellar spacing: 0.88 ± 0.01 nm, **Fig. 1**c; coating thickness: 24.35 μm, **Fig. S2** in SI). The particle size of MXene nanoflakes was characterized as 3277 ± 1233 nm (**Fig. S4**a) and its structure was further confirmed by XRD and Raman measurements (**Figs. S4**b and c in SI). The surface topography of the gear steel substrates was tailored by our developed CMP technology [18] (**Fig. 1**d), producing a series of surfaces with S_a ranging from 795 to 1.8 nm. **Fig. 1**e compares the corresponding evolution of the surface morphology, which clearly demonstrated the generation of a homogeneous, damage-free surface especially at the close-to-atomic scale.

Through the atomic-level polishing and atomic-level modification, tribological interfaces were established for subsequent friction tests. The average COF was evaluated over the same interval of 600–3600 s after the running-in stage for all tests. The results show that the average steady-state COF under the lubrication with IL and MXene coating at 300 ℃ is highly dependent on the pristine gear steel S_a. Notably, an ultra-low COF of approximately 0.01, indicative of an ultra-low friction state [44], was achieved under a high initial Hertzian contact pressure of 1.13 GPa, provided that the surface roughness S_a was below 58 nm (**Fig. 1**f). The ultra-low-friction behavior exhibited good reproducibility, as evidenced by four independent tests conducted under identical conditions at 300 °C, which yielded an overall average steady-state COF of 0.01149 ± 0.00058 (**Fig. S5**). This reproducible friction behavior further demonstrates the stable lubrication performance of IL/MXene-lubricated ball-on-disc tribological system under the present testing conditions. Moreover, this lubrication strategy enables the COF to remain stable within the range of 0.01–0.022 over a wide temperature range from RT to 300 °C, demonstrating its effectiveness and robustness across a broad temperature

Just Accepted

window (**Fig. S6**).

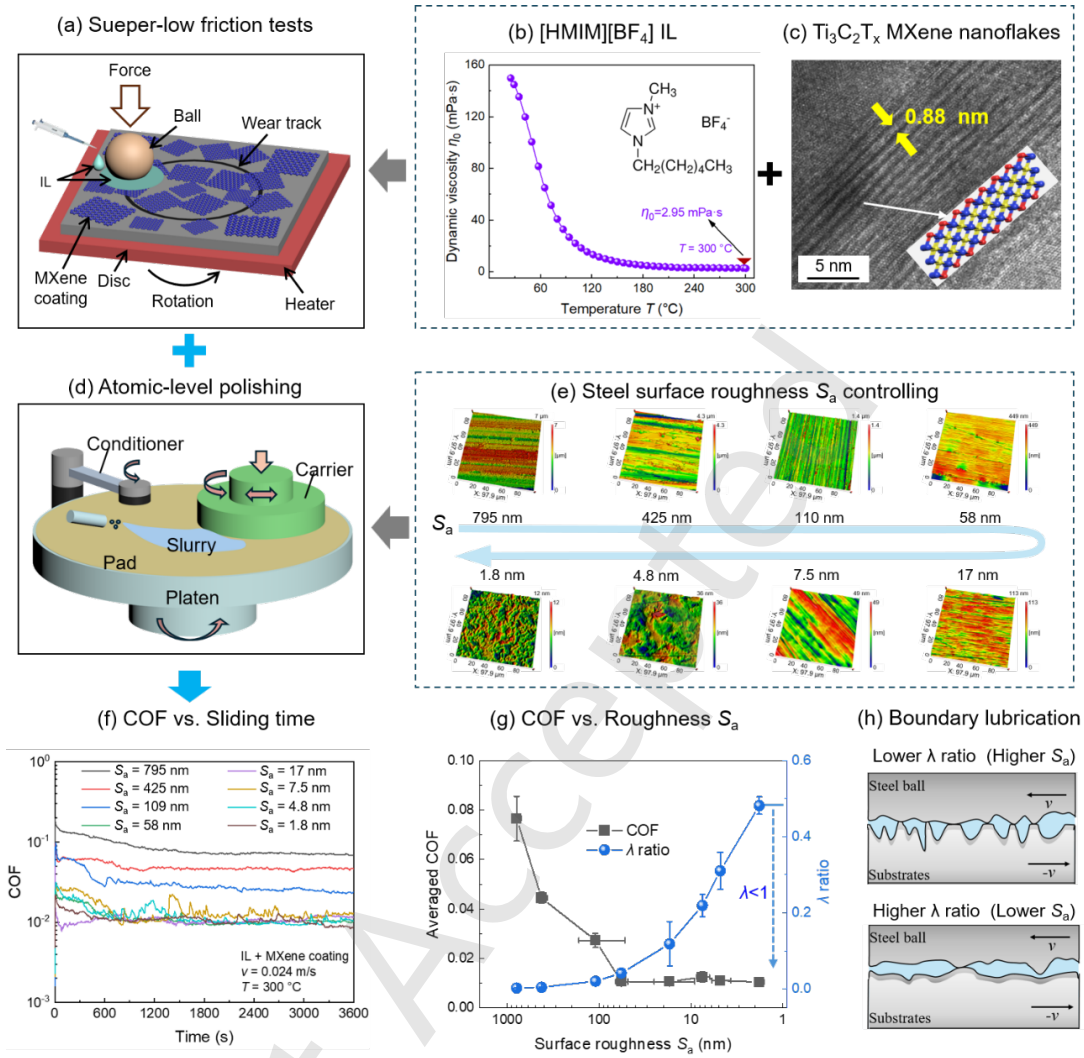


Fig. 1 Ultra-low friction at close-to-atomic scale surface roughness. (a) Schematic of a bearing steel ball rotationally sliding against an MXene-coated gear steel substrate lubricated with IL under temperature control. (b) Temperature-dependent dynamic viscosity and molecular structure of [HMIM][BF_4] IL. (c) TEM micrograph of $Ti_3C_2T_x$ MXene nanoflakes with the detected ~0.88 nm interlamellar spacing for monolayer (inset schematic diagram). (d) Schematic diagram of CMP device. (e) Steel surface roughness controlled from 795 nm to 1.8 nm *via* CMP. (f) COF versus sliding time for IL+MXene-lubricated steel discs with different S_a. (g) Steady-state COFs and calculated λ ratio as a function of surface roughness. (h) Boundary lubrication schematics of contact interface with various S_a.

The surface roughness-dependent average COF measured over the 600–3600 s steady-state interval (**Fig. 1**f) shows a continuous decrease with improving surface accuracy. This decreases plateaus when the substrate exhibits nanoscale roughness. Consequently, the lubrication regime, determined by substrate surface roughness, needs to be considered and can

Just Accepted

be characterized by the ratio λ of the calculated lubricant film thickness h [45] to the combined surface roughness [46]. In this regard, $\lambda < 1$ indicates boundary lubrication (BL), while $1 < \lambda < 3$ reflects mixed lubrication (ML), and $\lambda > 3$ stands for elastohydrodynamic lubrication (EHL).

$$\lambda = \frac{h}{\sqrt{\sigma_1^2 + \sigma_2^2}} \tag{3}$$

Here, σ_1 and σ_2 denoted the pre-wear zone roughness of the ball and disc, respectively [47-49]. The pre-wear roughness was adopted as it represents the prescribed pre-sliding surface states and provides a consistent reference for comparing nominal lubrication conditions, supporting the evaluation of surface parameters for engineering applications [50-52]. According to the Hamrock–Dowson theory, the central thickness h of the lubricating oil film between the tribo-pairs induced by the lubricants can be estimated as [45]:

$$h = 2.69U^{0.67}G^{0.53}RW^{-0.067}\left(1 - 0.61e^{-0.73k}\right) \tag{4}$$

$$U = \eta_0 u / E^* R \tag{5}$$

$$G = \kappa E^* \tag{6}$$

$$W = F_n / E^* R^2 \tag{7}$$

Here, η_0 is the dynamic viscosity of the IL at the actual testing temperature. For the tribological tests conducted at 300 °C, the experimentally measured value of η_0 = 2.95 mPa·s was used (**Fig. 1**b). u is the linear velocity. $E^* = 2/[(1\text{-}\nu_1^2)/E_1 + (1\text{-}\nu_2^2)/E_2] \approx 230.77$ GPa, where ν_i and E_i are Poisson's ratio and elastic modulus for each tribo-pair, respectively [39]. R is the radius of the GCr15 bearing steel ball [45, 53]. κ is the pressure-viscosity coefficient (11.91 GPa^{-1} [54]). F_n is the applied normal load (5 N). Ellipticity parameter k = 1.03.

Using the experimentally measured viscosity η_0 at 300 °C, the lubricant film thickness and λ values are determined. The lubricant film thickness is approximately 1.77 nm. Over the investigated surface roughness S_a range, all λ values remain below unity, indicating that the contact predominantly operates in the BL regime at 300 °C. It should also be noted that, in addition to the dynamic viscosity, the pressure–viscosity coefficient κ involved in the Hamrock–Dowson model has been reported to decrease with increasing temperature for ILs [55, 56]. Therefore, the actual lubricant film thickness at 300 °C may be lower than the present

Just Accepted

theoretical predictions, which would result in even smaller λ values. This indicates that the assignment of the contact to the BL regime remains robust.

Notably, λ increases progressively with decreasing S_a of the gear steel. Specifically, as the nominal S_a decreases from 795 nm to 17 nm and further to 1.8 nm, λ increases from 0.002 to 0.118 and 0.48, respectively, becoming approximately 59 and 240 times that of the roughest surface (**Fig. 1**g). Although λ remains below unity, its increase reflects an enhanced relative load-carrying capacity of the IL-based lubricating film, thereby promoting interfacial separation between the opposing surfaces and mitigating direct load-bearing asperity contacts [57, 58]. This more favorable interfacial condition contributes to the enhanced solid–liquid synergistic lubrication observed on the smoother surfaces. These results highlight surface-topography regulation as a key factor governing the attainment of ultra-low friction. However, the variation in λ alone cannot fully account for the pronounced friction reduction. Given the concurrent presence of IL and MXene at the sliding interface, their respective roles in the observed friction behavior require further elucidation.

3.2 Synergistic interplay of IL-MXene lubricants in ultra-low friction and wear

To decouple the contributions of the IL and MXene to ultra-low friction, we evaluated the steel substrates at 300 °C under an industrially relevant contact pressure (1.13 GPa) across four configurations: (1) pristine gear steel with a surface roughness around 17 nm, (2) MXene-coated, (3) IL-lubricated, and (4) MXene-coated with IL lubrication (denoted IL+MXene). Without any lubrication, the COF between the bare GCr15 and 18CrNiMo7-6 remained high at approximately 0.32 after running-in. When lubricated separately, the steady-state COF decreased to ~0.07 and ~0.03 for the MXene coating and the IL, respectively, after a shortened running-in time of about 300 s. In contrast, when the sliding interface was lubricated synergistically with both MXene and IL, an ultra-low friction state (0.01 COF) was achieved within a notably shorter running-in time of only ~80 s (**Fig. 2**a). Overall, the co-application of IL and MXene reduced the average COF by more than 28 times compared to the unlubricated pristine steel substrate (**Fig. 2**b).

Just Accepted

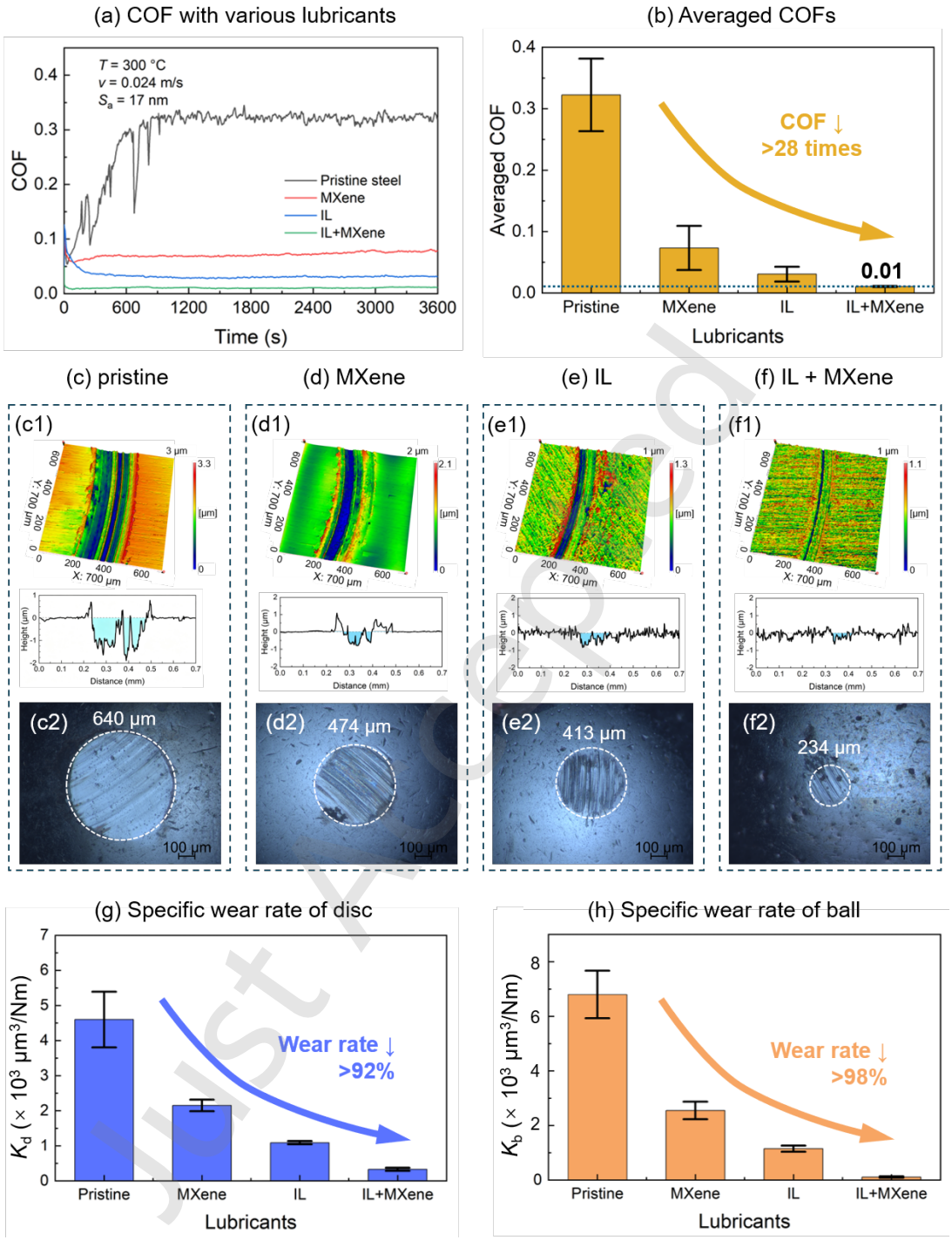


Fig. 2 Friction reduction and wear suppression *via* IL and MXene lubrication at 300°C. (a) Friction curves at 300 °C for pristine gear steel versus IL-lubricated, MXene-coated, and IL+MXene co-regulation. (b) Average steady-state COFs showing an approximately 28-fold reduction with IL+MXene versus pristine steel. (c-f) Wear track morphologies on gear steel discs with cross-sectional profiles (c1-f1) and corresponding ball wear scars (c2-f2). (g, h) Specific wear rate reductions exceeding 92% (gear steel substrate) and 98% (bearing steel counterface ball) under IL+MXene lubrication.

Just Accepted

Both materials notably mitigated surface wear on gear steel substrates (**Figs. 2**c1-f1) and bearing steel balls (**Figs. 2**c2-f2) when applied individually or synergistically. Notably, IL outperformed the MXene coating in the resulting lubrication efficacy (lower COF and wear), while the IL+MXene co-regulation delivered the best wear resistance, achieving 92.6% and 98.4% specific wear rate reductions for steel substrate (**Fig. 2**g) and counterpart steel balls (**Fig. 2**h), respectively. Such significant enhancement indicates that the lubrication performance of the tribological system arises from solid-liquid co-regulation rather than the simple superposition of lamellar interfaces and IL fluid film. This further highlights the significance of integrating low-shear-strength lamellar interfaces with the IL fluid film under extreme operating conditions, which may provide a practical route for extending the tribological performance beyond that achievable with either the liquid or solid lubricant alone. These results necessitate additional governing mechanisms beyond the IL-based fluid-film contribution and MXenes' low-shear properties to account for the observed ultra-low friction and wear resistance.

3.3 Atomic structure of the formed tribolayer depending on surface roughness

To elucidate the synergistic mechanism of the atomic-level polishing and modification under IL/MXene lubrication at 300 °C, TEM was performed on wear tracks of gear steel substrates. Focused ion beam (FIB) milling was used to prepare thin cross-sections from worn regions with a S_a of 17 nm (ultra-low friction state, COF ≈ 0.01) and 795 nm (COF ≈ 0.08), respectively. The TEM micrographs (**Figs. 3**a-b) reveal distinct tribolayers on both surfaces, with maximum thickness of ~470 nm on the smoother substrate with a roughness of 17 nm (I in **Fig. 3**a), approximately three times greater than that on the rougher surface (~160 nm at 795 nm roughness, I' in **Fig. 3**b). Although TEM characterization is limited to localized cross-sectional regions, the observed features adequately capture the characteristic differences in tribolayer architecture associated with surface roughness. Regarding the low surface roughness, the formed thicker tribolayer developed a multilayer architecture (II in **Fig. 3**a) that was comprised of a homogeneous upper layer (III) and a MXene-embedded bottom layer (IV and V). The HRTEM morphology in Fig. 3aVI and the selected-area electron diffraction (SAED) pattern in **Fig. 3**aVII confirmed MXenes' single-crystal orientation [59]. In contrast, the thinner

Just Accepted

tribolayer formed on the rougher surface contained a substantial dispersion of crystalline iron nanoparticles instead of MXene (**Figs. 3**bII'-V'), while HRTEM (**Fig. 3**bVI') and SAED (**Fig. 3**bVII') verified their nature and structure. Therefore, smoother steel surfaces promote more uniform amorphous tribolayer formation and enhance MXene transfer, constituting key mechanisms underlying friction reduction and wear resistance.

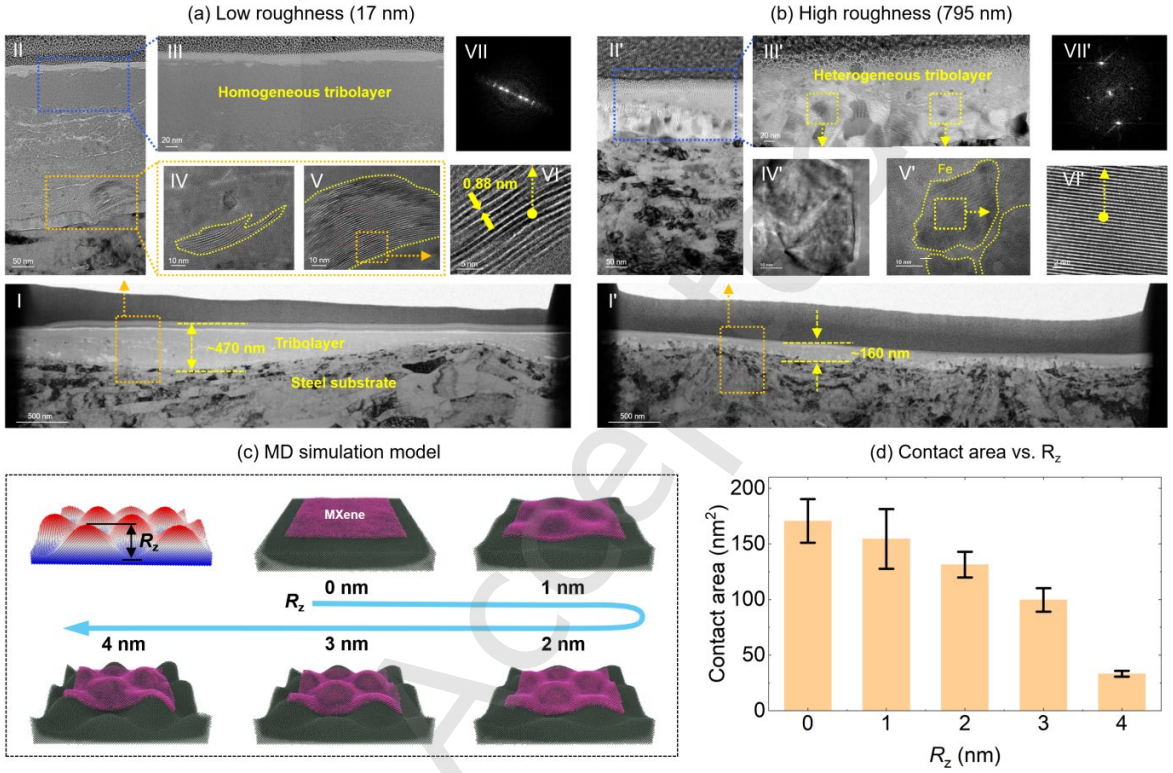


Fig. 3 Atomic structure and composition of tribolayers on contrasting steel substrates: correlative TEM and MD simulation analysis. (a,b) TEM images of FIB-prepared cross-sections showing a significantly thicker and more homogeneous tribolayer on the smooth steel substrate (S_a: 17 nm) than on the rough steel substrate (S_a: 795 nm). At low surface roughness, a tribolayer with maximum thickness up to ~470 nm (I) formed with a multilayer structure (II): a homogeneous upper phase (III) above a MXene-embedded layer (IV and V), as confirmed by HRTEM image (VI) and SAED pattern (VII). At high surface roughness, a ~160 nm thick tribolayer (I') dominated by heterogeneous phases (II' and III') embedded with Fe nanoparticles (IV' and V'), as characterized by corresponding HRTEM image (VI') and SAED pattern (VII'). (c) MD simulation models of MXene in contact with substrates of varying asperity heights (R_z) from 0 to 4 nm. (d) Simulated contact area between MXene and substrate versus R_z.

MD simulations modeled $Ti_3C_2T_x$ monolayers interacting with substrate surfaces having a controlled roughness to probe the atomic-scale retention mechanism. The surface topography was defined by R_z (0-4 nm), representing the asperity-to-base distance (**Fig. 3**c, please refer to

Methods). The MXene films deformed upon substrate contact, with interfacial contact area quantified through MXene deformation analysis. The simulation results indicated that an increased surface roughness greatly reduced the contact area between the MXene and substrate (**Fig. 3**d). This reduction is attributed to the stiffness of MXene, which causes it to delaminate from steep surface asperities, thereby weakening interfacial adhesion [60, 61]. This suggests more favorable interfacial conformity/retention of MXene on smoother substrates (**Fig. 3**c), ultimately tailoring the lubrication performance through friction reduction and wear suppression.

3.4 Atomic mechanism of IL/MXene synergistic lubrication at elevated temperature

TEM-EDS mapping depicted in **Fig. 4** compared the chemical composition of formed tribolayers on the steel substrates with surface roughness of (a) 17 and (b) 795 nm, respectively. It further reveals the divergent tribolayer thicknesses on these two steel surfaces. An inverse correlation between O-enrichment and Fe-depletion signals confirms temperature-driven oxidation. Additionally, the distinct Ti signal is expected to originate from MXenes, while F signal variations stem from IL but B remained undetectable in this analysis. The EDS results provide direct evidence for the tribolayers' origin, demonstrating that its formation is attributed to shear-induced reactions between the steel substrate, IL, and MXene coating.

The XPS analysis within the tribo-pair contact zone helped to further elucidate the tribolayers' chemical evolution. As for the Fe 2p spectrum (**Fig. 4**c), according to the position of the primary and satellite peak of Fe $2p_{3/2}$, it can be judged that the metallic Fe has been completely transformed to Fe^{3+} [62, 63], including FeF_3 and Fe_2O_3 (Fe 2p in **Fig. S7**a). At 300°C, these Fe^{3+} reacted products (**Figs. 4**c and d) form robustly independent of surface roughness. The F 1s and B 1s spectra **(Figs. S7**b and c) only display signals belonging to FeF_3 and B_2O_3, respectively [64, 65]. These species originated from the oxidation and decomposition of the anion $[BF_4]^-$ in the IL. Furthermore, two peaks of the Ti 2p spectrum (**Fig. S7**d) illustrate the MXene breakdown and TiO_2 formation [66, 67]. The disappearance of the C-Ti bonds

Just Accepted

located at 281.9-282.1 eV in C 1s spectrum (**Fig. S7**e) implies the complete decomposition of $Ti_3C_2T_x$ [68, 69]. The characteristic peak at 529.9 eV in the O1s spectrum (**Fig. S7**f) can be ascribed to metal oxides, potentially encompassing compounds such as iron oxide and titanium oxide. Spectral signals of other elements (e.g., Cr, Ni, and Mo) do not manifest discernible peaks (**Figs. S7**g-i), due to the relatively low content (3.15–3.85 wt.% in total [39, 70]).

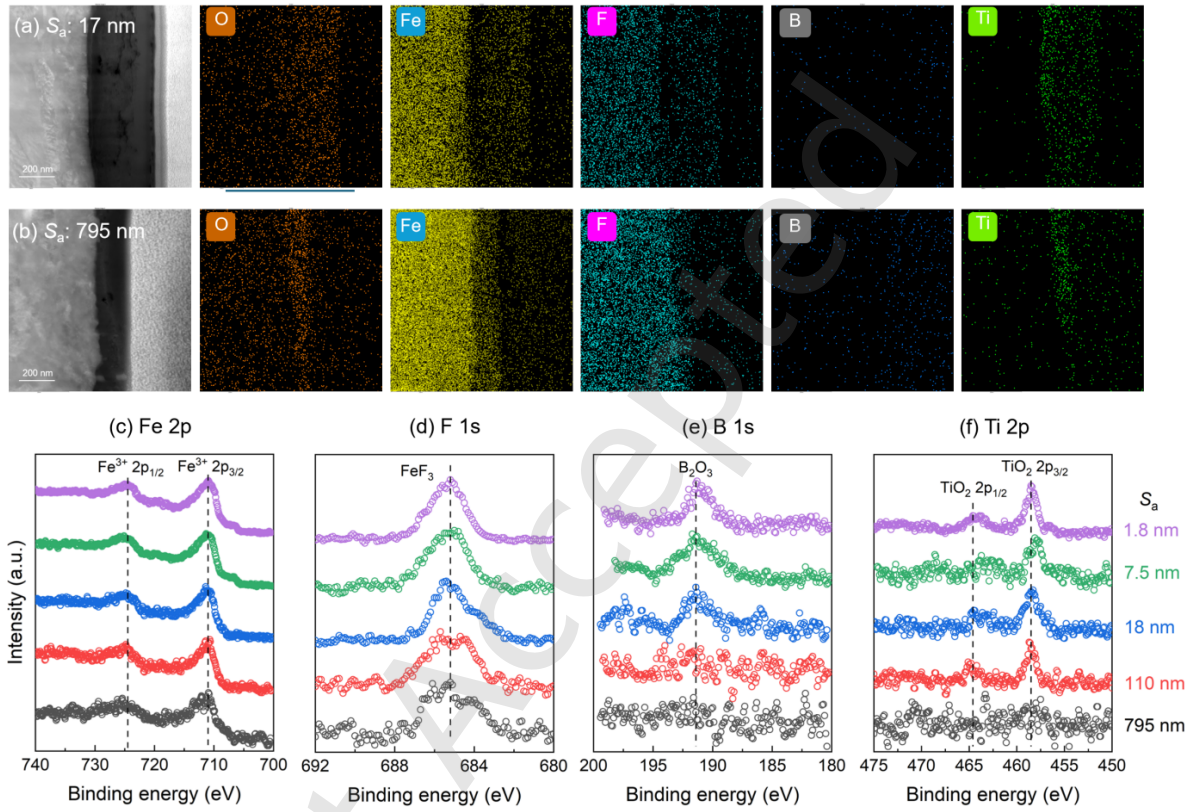


Fig. 4 Dependence of tribolayer composition on steel substrate surface roughness. (a,b) TEM-EDS elemental maps of tribolayers corresponding to regions in (a) and (b), showing distributions of O, Fe, F, B, and Ti. (c-f) XPS analysis of wear tracks on steel substrates with different roughness. (c) Fe 2p. (d) F 1s. (e) B 1s. (f) Ti 2p.

Different from that of Fe^{3+} reacted products (**Figs. 4**c and d), the effective formation of a stable B_2O_3-TiO_2-containing composite film-essential for friction reduction requires the disc surface roughness to be reduced to nanoscale or even near-atomic scale (**Figs. 4**e and f). A higher roughness compromises film adhesion due to increased residual stresses from localized strain at asperities, leading to film cracking and delamination [71, 72]. Consequently, achieving ultra-low friction is contingent upon the formation of a complete and coherent composite

Just Accepted

lubricious film.

In summary, the sliding of steel interface lubricated with IL and MXene coating strongly depends on the substrate roughness (**Figs. 5**a and b). Considering the synergistic friction reduction by B_2O_3/FeF_3 (documented in IL tribology [73]) and TiO_2's solid lubricant functionality [74], combined with Fe_2O_3's intrinsic low-friction behavior [75, 76], ultra-low friction and wear can be achieved under BL. This is attributed to: (1) the IL-based fluid film contributes to interfacial separation and mitigates direct load-bearing asperity contacts (**Figs. 5**c and d), and (2) MXene-embedded B_2O_3-FeF_3-TiO_2-Fe_2O_3 nanocomposite that reduces the acting interfacial shear while protecting the steel substrate (**Fig. 5**c and e). Critically, the adhesion of MXene nanosheets (Right inset in **Fig. 5**c) and formation of stable B_2O_3-TiO_2 components in tribolayer require nanoscale and even atomic-scale surface roughness (**Figs. 4**e and f), underscoring the significant role of ultra-precision surface manufacturing in friction and wear control.

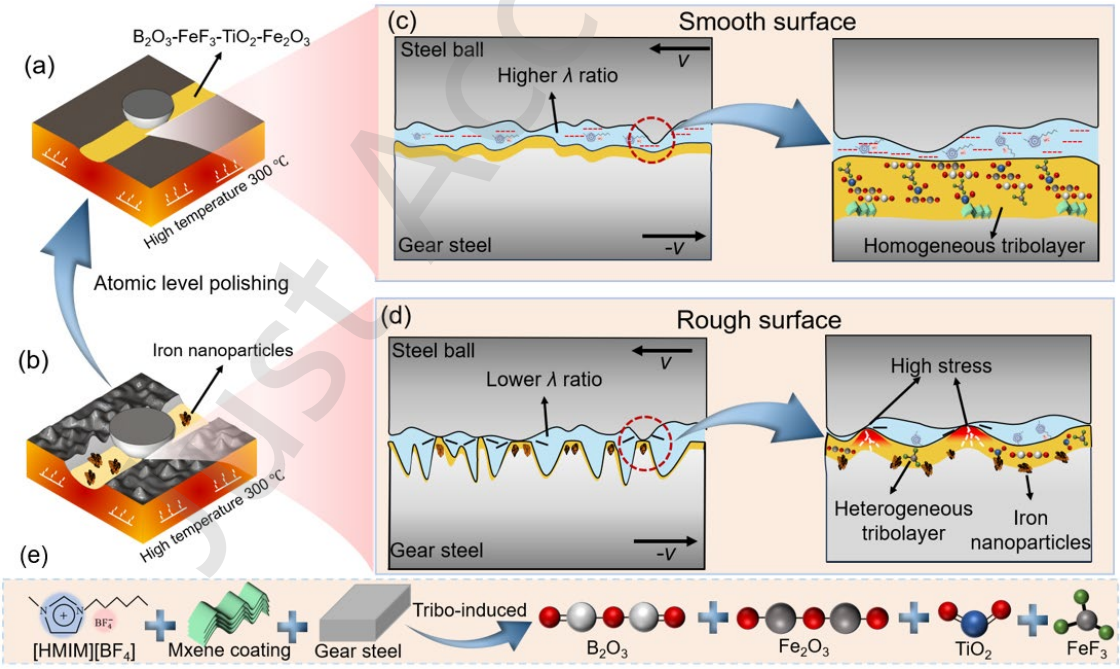


Fig. 5 Schematic illustration of the solid-liquid synergistic lubrication depending on the surface roughness. (a, b) Sliding on smooth and rough steel surfaces at a temperature of 300 °C. (c) Lubrication mechanism on the close-to-atomic smooth surface: BL with a higher λ ratio and formation of thick homogeneous tribolayer with adhesion of MXene layer on the steel substrate. (d) Lubrication mechanism on the rough surface: BL with a lower λ ratio and formation of thin heterogeneous tribolayer. (e) Formation of B_2O_3-FeF_3-TiO_2-Fe_2O_3 nanocomposite.

Just Accepted

The above findings further confirm that integrating atomic-level polishing as well as atomic-level modifications *via* 2D material coating and IL constitutes an effective approach for achieving ultra-low friction and wear resistance at the tribological interface in engineering applications. The proposed solid-liquid synergy provides a rational route for constructing robust lubrication interfaces by regulating load-bearing asperity contacts, coating adhesion, and tribofilm formation under extreme conditions. The effectiveness of this synergistic lubrication strategy is further demonstrated by comparison with the reported lubrication systems. Given the differences in materials and testing conditions (**Table S1**), the comparison should be regarded as a general performance reference rather than a rigorous quantitative comparison. Even so, the present tribological system exhibits competitive friction performance compared with reported traditional oil-based [6, 8, 10, 77, 78] and IL-based [25-28, 79-84] lubrication systems within the temperature range of 100–300 °C (**Fig. 6**). Although ultra-low friction has been achieved in the present study, further performance enhancements may be realized by optimizing the MXene nanoflake size, coating deposition techniques, together with tailored control of the S_a of the counterpart steel ball. Future systematic studies of these parameters will be essential for further advancing the friction-reduction capability, wear resistance, and overall robustness of the tribological system.

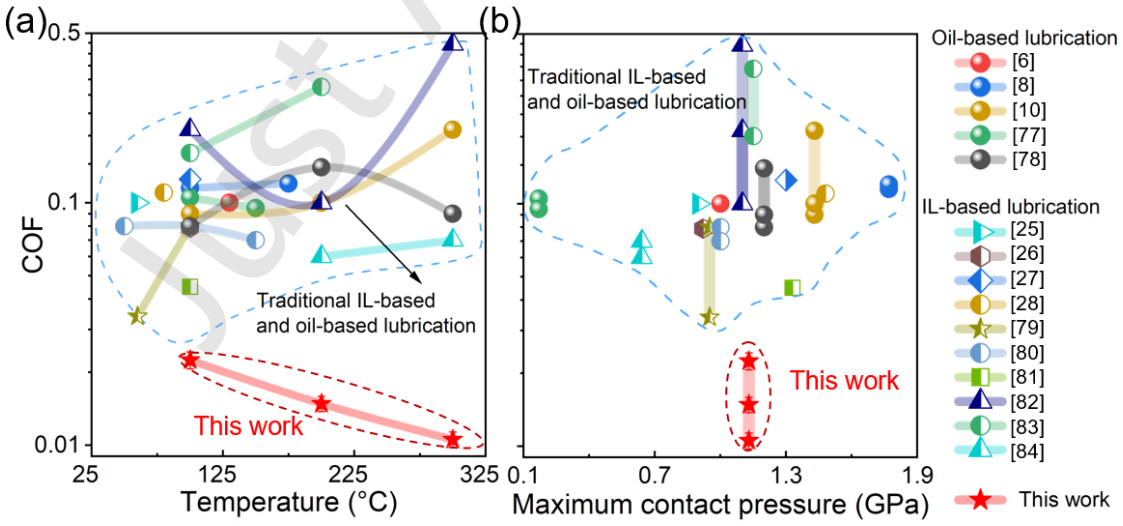


Fig. 6 A summary of existing literature on oil-based lubrication and ionic liquid lubrication. (a) COF versus temperature. (b) COF versus the maximum Hertzian contact pressure. The detailed material combinations and tribological test conditions corresponding to the literature data are summarized in **Table S1**.

Just Accepted

4. Conclusion

This study establishes a solid-liquid synergistic lubrication strategy, combining atomic-level polishing with an IL ([HMIM][BF_4]) and a MXene coating, to achieve ultra-low friction (~0.01 COF) on steel-steel interfaces at elevated temperature (300 °C) under high contact pressure (>1.1 GPa). Through tribo-testing, materials characterization and MD simulations, the effect of surface roughness was systematically elucidated. The results demonstrate that ultra-low friction is achieved within the BL regime through the concurrent action of the low-shear lamellar interfaces and the IL-based fluid film. The smoother steel substrate promotes interfacial separation between the opposing surfaces and mitigates direct load-bearing asperity contacts, thereby enhancing solid–liquid synergistic lubrication. MD simulations provided qualitative atomic-scale insights into how nanoscale surface smoothness favors the interfacial conformity and retention of MXene. TEM and XPS characterization further demonstrated that the smoother surface facilitates the formation of a thicker, more homogeneous, and protective B_2O_3–FeF_3–TiO_2–Fe_2O_3-containing composite tribofilm. This lubrication strategy is expected to accelerate the adoption of atomic-level polishing, lamellar materials and IL into liquid lubrication to overcome the lubrication failure challenge and translate into commercial applications, as well as provide new insights into the rational design of high-performance lubrication systems for extreme conditions.

Just Accepted

Acknowledgements:

This work was supported by the Sichuan Science and Technology Program (No. 2025ZDZX0028), the National Natural Science Foundation of China (Grant Nos. 92580208 and 52235004), and the China Scholarship Council. The authors gratefully acknowledge the financial support of ANID-Chile within the projects Fondecyt Regular 1220331 and Fondequip EQM190057 as well as the Millennium Science Initiative Program (NCN2023_007). We would like to thank the Analytical and Testing Center of Southwest Jiaotong University for the SEM/EDS tests.

Declaration of Competing Interest

The authors declare that they have no known competing financial interests or personal relationships that could have appeared to influence the work reported in this paper.

References

[1] Holmberg K, Erdemir A, Influence of tribology on global energy consumption, costs and emissions. *Friction* **5**(3): 263-284 (2017)

[2] Zaretsky E V, Liquid lubrication in space. *Tribol Int* **23**(2): 75-93 (1990)

[3] Höhn B R, Michaelis K, Influence of oil temperature on gear failures. *Tribol Int* **37**(2): 103-109 (2004)

[4] Wu C H, Kung Y T, A parametric study on oil/air lubrication of a high-speed spindle. *Precis Eng* **29**(2): 162-167 (2005)

[5] Du C, Sheng C, Liang X, Rao X, Guo Z, Effects of temperature on the tribological properties of cylinder-liner piston ring lubricated with different oils. *Lubricants* **11**(3): 115 (2023)

[6] Wang Y, Qiu Q, Zhang P, Gao X, Zhang Z, Huang P, Correlation between lubricating oil characteristic parameters and friction characteristics. *Coatings* **13**(5): 881 (2023)

[7] Fan X, Xue Q, Wang L, Carbon-based solid-liquid lubricating coatings for space applications-A review. *Friction* **3**(3): 191-207 (2015)

[8] Cai Z B, Zhou Y, Qu J, Effect of oil temperature on tribological behavior of a lubricated steel−steel contact. *Wear* **332-333**: 1158-1163 (2015)

[9] Meng Y, Wen X, Cheng J, Bai P, Meng Y, Tian Y, High temperature lubrication performance of chlorophenyl silicone oil. *Friction* **12**(8): 1716-1727 (2024)

[10] Ye P, Jiang X, Li S, Li S, Preparation of $NiMoO_2S_2$ nanoparticle and investigation of its tribological behavior as additive in lubricating oils. *Wear* **253**(5): 572-575 (2002)

[11] Erdemir A, Ramirez G, Eryilmaz O L, Narayanan B, Liao Y, Kamath G, Sankaranarayanan S K, Carbon-based tribofilms from lubricating oils. *Nature* **536**(7614): 67-71 (2016)

[12] Macknojia A, Ayyagari A, Zambrano D, Rosenkranz A, Shevchenko E V, Berman D, Macroscale superlubricity induced by MXene/MoS_2 nanocomposites on rough steel surfaces under high contact stresses. *ACS Nano* **17**(3): 2421-2430 (2023)

[13] Wang B, Gao K, Chang Q, Berman D, Tian Y, Magnesium silicate hydroxide–MoS_2–Sb_2O_3 coating nanomaterials for high-temperature superlubricity. *ACS Appl Nano Mater* **4**(7): 7097-7106 (2021)

[14] Zhai W, Zhou K, Nanomaterials in superlubricity. *Adv Funct Mater* **29**(28): 1806395 (2019)

[15] Ge X, Li J, Luo J, Macroscale superlubricity achieved with various liquid molecules: A review. *Front Mech Eng* **5**: 2 (2019)

[16] Dang S, Xiao C, Li J, Jiang Y, Franklin S E, Qian L, Chen L, Achieving highly selective polishing of polysilicon over oxide and nitride films via ethylenediamine-modulated interfacial mechanochemistry. *J Manuf Process* **156**: 497-508 (2025)

[17] Chen L, Wen J, Zhang P, Yu B, Chen C, Ma T, Lu X, Kim S H, Qian L, Nanomanufacturing of silicon surface with a single atomic layer precision via mechanochemical reactions. *Nat Commun* **9**(1): 1542 (2018)

[18] Peng W, Gao Y, Jiang L, Liu J, Qian L, Attaining ultra-smooth 18CrNiMo7-6 case hardening steel surfaces

Just Accepted

with chemical mechanical polishing. *Lubricants* **10**(9): 199 (2022)
[19] Zhu D, Jane Wang Q, Effect of roughness orientation on the elastohydrodynamic lubrication film thickness. *J Tribol* **135**(3): 031501 (2013)
[20] Zhu D, Wang J, Ren N, Wang Q J, Mixed elastohydrodynamic lubrication in finite roller contacts involving realistic geometry and surface roughness. *J Tribol* **134**(1): 011504 (2012)
[21] Rahman M M, Islam M, Roy R, Younis H, AlNahyan M, Younes H, Carbon nanomaterial-based lubricants: review of recent developments. *Lubricants* **10**(11): 281 (2022)
[22] Mannix A J, Kiraly B, Hersam M C, Guisinger N P, Synthesis and chemistry of elemental 2D materials. *Nat Rev Chem* **1**(2): 0014 (2017)
[23] Liu Y, Weiss N O, Duan X, Cheng H-C, Huang Y, Duan X, Van der Waals heterostructures and devices. *Nat Rev Mater* **1**(9): 16042 (2016)
[24] Satterthwaite P F, Zhu W, Jastrzebska-Perfect P, Tang M, Spector S O, Gao H, Kitadai H, Lu A-Y, Tan Q, Tang S-Y, Van der Waals device integration beyond the limits of van der Waals forces using adhesive matrix transfer. *Nat Electron* **7**(1): 17-28 (2024)
[25] Millar W, Aman Z M, Atkin R, Li H, Graphite infused ionic liquid greases. *Colloids Surf, A* **653**: 130017 (2022)
[26] Jiménez A E, Bermúdez M D, Carrión F J, Martínez-Nicolás G, Room temperature ionic liquids as lubricant additives in steel–aluminium contacts: Influence of sliding velocity, normal load and temperature. *Wear* **261**(3): 347-359 (2006)
[27] García A, González R, Hernández Battez A, Viesca J L, Monge R, Fernández-González A, Hadfield M, Ionic liquids as a neat lubricant applied to steel–steel contacts. *Tribol Int* **72**: 42-50 (2014)
[28] Yan J, Lien H M, Mangolini F, Linking molecular structure and lubrication mechanisms in tetraalkylammonium orthoborate ionic liquids. *Tribol Lett* **71**(2): 41 (2023)
[29] Minami I, Ionic liquids in tribology. *Molecules* **14**(6): 2286-2305 (2009)
[30] Jimenez A E, Bermúdez M D, Ionic liquids as lubricants for steel–aluminum contacts at low and elevated temperatures. *Tribol Lett* **26**(1): 53-60 (2007)
[31] Saurín N, Minami I, Sanes J, Bermúdez M, Study of the effect of tribo-materials and surface finish on the lubricant performance of new halogen-free room temperature ionic liquids. *Appl Surf Sci* **366**: 464-474 (2016)
[32] Liu L, Zhou M, Jin L, Li L, Mo Y, Su G, Li X, Zhu H, Tian Y, Recent advances in friction and lubrication of graphene and other 2D materials: Mechanisms and applications. *Friction* **7**(3): 199-216 (2019)
[33] Wang P, Liang H, Jiang L, Qian L, Effect of nanoscale surface roughness on sliding friction and wear in mixed lubrication. *Wear* **530**: 204995 (2023)
[34] Wang W, Chen H, Hu Y, Wang H, Effect of surface roughness parameters on mixed lubrication characteristics. *Tribol Int* **39**(6): 522-527 (2006)
[35] Liu Y, Wang Y, Hou J, Shen W, Zhang X, Li Z, Li P, Fu X, Wang Y, Wu C, Improved tribological properties of MXene nanosheet filler-modified PPO composites. *J Colloid Interface Sci* **680**: 618-631 (2025)
[36] Rosenkranz A, Righi M C, Sumant A V, Anasori B, Mochalin V N, Perspectives of 2D MXene Tribology. *Adv Mater* **35**(5): e2207757 (2023)
[37] Feng Q, Dou M, Yang J, Zou S, Li Z, Wei L, Huang F, Heterostructures Comprised of MXene Nanosheets for Tribology: A Review. *ACS Appl Nano Mater* **7**(19): 22379-22416 (2024)
[38] Piljević M, Ostermann M, Marquis E, Schwarz S, Stöger-Pollach M, Gogotsi O, Valtiner M, Rodríguez Ripoll M, Gachot C, Bilotto P, Electrochemically synthesized MXenes as sustainable solid lubricants: Mechanistic insights into tribofilm formation and interfacial dynamics. *Carbon* **248**: 121136 (2026)

Just Accepted

[39] Liu Y, Chen L, Wang Y, Qian L, Combined effect of WS_2 and $Ti_3C_2T_x$ MXene favors oil-based ultra-low friction on rough steel-steel interface at elevated temperatures. *Sci China Technol Sci* **67**(7): 1991-2002 (2024)
[40] Archard J, Contact and rubbing of flat surfaces. *J Appl Phys* **24**(8): 981-988 (1953)
[41] Plummer G, Tucker G J, Bond-order potentials for the Ti_3AlC_2 and Ti_3SiC_2 MAX phases. *Phys Rev B* **100**(21): 214114 (2019)
[42] Aktulga H M, Fogarty J C, Pandit S A, Grama A Y, Parallel reactive molecular dynamics: Numerical methods and algorithmic techniques. *Parallel Comput* **38**(4-5): 245-259 (2012)
[43] Stukowski A, Visualization and analysis of atomistic simulation data with OVITO–the Open Visualization Tool. *Modell Simul Mater Sci Eng* **18**(1): 015012 (2010)
[44] Liu C, Shao J, Zhang J, Wong J S S, Meng Y, Zeng H, Tian Y, The Last Dance of Lubrication: Capturing Ultralow Friction before Full Evaporation. *Nano Lett* **25**(28): 11019-11026 (2025)
[45] Hamrock B J, Dowson D, Isothermal Elastohydrodynamic Lubrication of Point Contacts: Part III—Fully Flooded Results. *J Lubr Technol* **99**(2): 264-275 (1977)
[46] Tallian T E, On Competing Failure Modes in Rolling Contact. *ASLE Trans* **10**(4): 418-439 (1967)
[47] Taylor R I, Sherrington I, Estimating Mixed & Boundary Friction from the Lambda Ratio: Incorporating the Effect of Surface Character. *Tribol Trans* **69**(1): 134-141 (2026)
[48] Esmaeili K, Wang L, Harvey T J, White N M, Holweger W, A study on the influence of electrical discharges on the formation of white etching cracks in oil-lubricated rolling contacts and their detection using electrostatic sensing technique. *Lubricants* **11**(4): 164 (2023)
[49] Reitschuster S, Maier E, Lohner T, Stahl K, Bobzin K, Kalscheuer C, Thiex M, Sperka P, Hartl M, DLC-Coated Thermoplastics: Tribological Analyses under Lubricated Rolling-Sliding Conditions. *Tribol Lett* **70**(4): 121 (2022)
[50] Johansson P, Marklund P, Björling M, Shi Y, Effect of roughness on the running-in behavior and tribofilm formation of carbon fiber reinforced PTFE composite in trace moisture environment. *Wear* **500-501**: 204367 (2022)
[51] Vrček A, Hultqvist T, Baubet Y, Björling M, Marklund P, Larsson R, Micro-Pitting and Wear Assessment of PAO vs Mineral-Based Engine Oil Operating under Mixed Lubrication Conditions: Effects of Lambda, Roughness Lay and Sliding Direction. *Lubricants* **7**(5): 42 (2019)
[52] Spies C, Parab Y, Fatemi A, Mixed friction: Critical assessment of engineering load sharing equations based on the Lambda-parameter. *Tribol Int* **211**: 110812 (2025)
[53] Cyriac F, Lugt P M, Bosman R, Padberg C J, Venner C H, Effect of Thickener Particle Geometry and Concentration on the Grease EHL Film Thickness at Medium Speeds. *Tribol Lett* **61**(2): 18 (2016)
[54] Ahosseini A, Scurto A M, Viscosity of imidazolium-based ionic liquids at elevated pressures: cation and anion effects. *Int J Thermophys* **29**(4): 1222-1243 (2008)
[55] Regueira T, Lugo L, Comuñas M a J P, Fernández J, High Pressure Rheological Behavior of 1-Ethyl-3-methylimidazolium n-Hexylsulfate and Trihexyl(tetradecyl)phosphonium Tris(pentafluoroethyl)trifluorophosphate. *J Chem Eng Data* **62**(9): 2927-2936 (2017)
[56] Pensado A S, Comuñas M J P, Fernández J, The Pressure–Viscosity Coefficient of Several Ionic Liquids. *Tribol Lett* **31**(2): 107-118 (2008)
[57] Zhu D, Wang Q J, On the λ ratio range of mixed lubrication. *Proc Inst Mech Eng, Part J* **226**(12): 1010-1022 (2012)
[58] Cann P, Ioannides E, Jacobson B, Lubrecht A, The lambda ratio—a critical re-examination. *Wear* **175**(1-2): 177-188 (1994)
[59] Naguib M, Mashtalir O, Carle J, Presser V, Lu J, Hultman L, Gogotsi Y, Barsoum M W, Two-dimensional

Just Accepted

transition metal carbides. *ACS nano* **6**(2): 1322-1331 (2012)
[60] Cullen W G, Yamamoto M, Burson K M, Chen J-H, Jang C, Li L, Fuhrer M S, Williams E D, High-fidelity conformation of graphene to SiO_2 topographic features. *Phys Rev Lett* **105**(21): 215504 (2010)
[61] Makumi S W, Aksamija Z, Impact of Substrate Roughness on the Thermal Boundary Conductance in 2D Materials. *J Phys Chem C* **129**(14): 6991-6999 (2025)
[62] Yamashita T, Hayes P, Analysis of XPS spectra of Fe^{2+} and Fe^{3+} ions in oxide materials. *Appl Surf Sci* **254**(8): 2441-2449 (2008)
[63] Biesinger M C, Payne B P, Grosvenor A P, Lau L W, Gerson A R, Smart R S C, Resolving surface chemical states in XPS analysis of first row transition metals, oxides and hydroxides: Cr, Mn, Fe, Co and Ni. *Appl Surf Sci* **257**(7): 2717-2730 (2011)
[64] Jiménez A, Bermúdez M, Iglesias P, Lubrication of Inconel 600 with ionic liquids at high temperature. *Tribol Int* **42**(11-12): 1744-1751 (2009)
[65] Ye C, Liu W, Chen Y, Yu L, Room-temperature ionic liquids: a novel versatile lubricant. *Chem Commun* (21): 2244-2245 (2001)
[66] Kuznetsov M, Zhuravlev J F, Gubanov V, XPS analysis of adsorption of oxygen molecules on the surface of Ti and TiN_x films in vacuum. *J Electron Spectrosc Relat Phenom* **58**(3): 169-176 (1992)
[67] Boffa A, Galloway H, Jacobs P, Benitez J, Batteas J, Salmeron M, Bell A, Somorjai G A, The growth and structure of titanium oxide films on Pt (111) investigated by LEED, XPS, ISS, and STM. *Surf Sci* **326**(1-2): 80-92 (1995)
[68] Natu V, Benchakar M, Canaff C, Habrioux A, Célérier S, Barsoum M W, A critical analysis of the X-ray photoelectron spectra of $Ti_3C_2T_z$ MXenes. *Matter* **4**(4): 1224-1251 (2021)
[69] Näslund L-Å, Persson I, XPS spectra curve fittings of $Ti_3C_2T_x$ based on first principles thinking. *Appl Surf Sci* **593**: 153442 (2022)
[70] Stickel D, Fischer A, The influence of topography on the specific dissipated friction power in ultra-mild sliding wear: Experiment and simulation. *Tribol Int* **91**: 48-59 (2015)
[71] Li H, Contryman A W, Qian X, Ardakani S M, Gong Y, Wang X, Weisse J M, Lee C H, Zhao J, Ajayan P M, Optoelectronic crystal of artificial atoms in strain-textured molybdenum disulphide. *Nat Commun* **6**(1): 7381 (2015)
[72] Ostadi A, Hosseini S H, Fordoei M E, The effect of temperature and roughness of the substrate surface on the microstructure and adhesion strength of EB-PVD ZrO_2-% 8wtY_2O_3 coating. *Ceram Int* **46**(2): 2287-2293 (2020)
[73] Liu W, Ye C, Gong Q, Wang H, Wang P, Tribological performance of room-temperature ionic liquids as lubricant. *Tribol Lett* **13**(2): 81-85 (2002)
[74] Han K, Ma L, Tian Y, Luo J, Photoinduced superlubricity on TiO_2 surfaces. *Friction* **12**(3): 428-438 (2024)
[75] Ge X, Halmans T, Li J, Luo J, Molecular behaviors in thin film lubrication—Part three: Superlubricity attained by polar and nonpolar molecules. *Friction* **7**(6): 625-636 (2019)
[76] Chen M M, Lin J, Wu T W, Castillo G, Wear resistance of iron oxide thin films. *J Appl Phys* **63**(8): 3275-3277 (1988)
[77] Ruan H, Zhang Y, Li S, Yang L, Wang C, Wang T, Wang Q, Effect of temperature on the friction and wear performance of porous oil-containing polyimide. *Tribol Int* **157**: 106891 (2021)
[78] Zhu L, Dong J, Zeng Q, High temperature solid/liquid lubrication behaviours of DLC films. *Lubr Sci* **33**(5): 229-245 (2021)
[79] Sernaglia M, Blanco D, Battez A H, Viesca J L, González R, Bartolomé M, Two fatty acid anion-based ionic

Just Accepted

liquids - part I: Physicochemical properties and tribological behavior as neat lubricants. *J Mol Liq* **305**: 112827 (2020)
[80] Pejaković V, Kronberger M, Kalin M, Influence of temperature on tribological behaviour of ionic liquids as lubricants and lubricant additives. *Lubr Sci* **26**(2): 107-115 (2014)
[81] Reeves C J, Kasar A K, Menezes P L, Tribological performance of environmental friendly ionic liquids for high-temperature applications. *J Cleaner Prod* **279**: 123666 (2021)
[82] Jiménez A E, Bermúdez M D, Ionic Liquids as Lubricants of Titanium–Steel Contact. Part 2: Friction, Wear and Surface Interactions at High Temperature. *Tribol Lett* **37**(2): 431-443 (2010)
[83] Bermúdez M, Jiménez A, Surface interactions in lubrication of titanium, aluminium, and titanium–aluminium alloys with the ionic liquid [C_2mim] Tf_2N under increasing temperature. *Proc Inst Mech Eng, Part J* **226**(11): 977-990 (2012)
[84] Hatsuda K, Kondo H, Murakami T, Effect of a long alkyl chain in protic ionic liquids molecules on tribological properties at high temperature. *Tribol Online* **15**(5): 356-364 (2020)

Biography of the corresponding author:



Lei CHEN. He is a professor of mechanical engineering at Southwest Jiaotong University, China. He received his Ph.D. degree from Southwest Jiaotong University in 2013. He acted as a visiting scholar from 2016 to 2017 in The Pennsylvania State University, USA. He has a background in mechanical engineering and surface science. His current research interest includes atomic-level polishing, atomic-level modification. He can be reached at chenlei@swjtu.edu.cn.

Biography of the first author:

Just Accepted



Shehui DANG. He received his bachelor's degree in mechanical engineering in 2021 from Dalian Jiaotong University, China. He is currently a Ph.D. candidate in mechanical engineering at Southwest Jiaotong University, China. His research interest includes chemical mechanical polishing and nanotribology.

Just Accepted